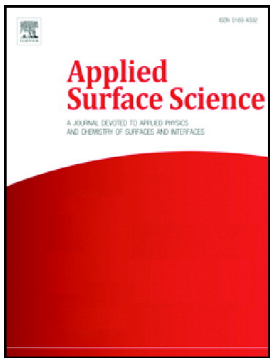

Quality improvement of CZTS thin films deposited by spray pyrolysis method using pulsed Nd: YAG laser irradiation

A. Shamardin, D. Kurbatov, L. Grase, J. Vecstaudža, J. Kaupužs, A. Medvids

PII: S0169-4332(19)31635-6
DOI: https://doi.org/10.1016/j.apsusc.2019.05.315
Reference: APSUSC 42902

To appear in: *Applied Surface Science*

Received date: 18 January 2019
Revised date: 3 May 2019
Accepted date: 27 May 2019

Please cite this article as: A. Shamardin, D. Kurbatov, L. Grase, et al., Quality improvement of CZTS thin films deposited by spray pyrolysis method using pulsed Nd: YAG laser irradiation, Applied Surface Science, https://doi.org/10.1016/j.apsusc.2019.05.315

Quality Improvement of CZTS Thin Films Deposited by Spray Pyrolysis Method Using Pulsed Nd: YAG Laser Irradiation

A. Shamardin[1], D. Kurbatov[1], L. Grase[2], J. Vecstaudža[3], J. Kaupužs[4], A. Medvids[4]

1) Faculty of Electronics and Information Technology, Department of Electronics and Computer Technology, Sumy State University, 2, Rymskogo-Korsakova st., 40007, Sumy, Ukraine

2) Institute of Silicate Materials, Faculty of Materials Science and Applied Chemistry, Riga Technical University, P. Valdena 3/7, Riga, LV-1048, Latvia

3) Rudolfs Cimdins Riga Biomaterials Innovations and Development Centre of RTU, Institute of General Chemical Engineering, Faculty of Materials Science and Applied Chemistry, Riga Technical University, Pulka Str 3, Riga, LV-1007, Latvia

4) Institute of Technical Physics, Faculty of Materials Science and Applied Chemistry, Riga Technical University, P. Valdena 3/7, Riga, LV-1048, Latvia

Corresponding Author: **Artem Shamardin**

Sumy State University, Faculty of Electronics and Information Technology, Department of Electronics and Computer Technology

2, Rymskogo-Korsakova st., 40007, Sumy, Ukraine

Tel.: +380939405058

E-mail: artemv.shamardin@gmail.com

Abstract

In this work, thin films of Cu_2ZnSnS_4 (CZTS) were grown by spray-pyrolysis method and were irradiated by pulsed Nd: YAG laser. Their morphological, chemical, structural and substructural characteristics were investigated using AFM, SEM, EDS, XRD and Raman spectroscopy. Upon laser irradiation, improvement of crystallinity, stoichiometry and surface morphology were observed in the obtained CZTS thin films with the normal distribution of newly-formed particles throughout the plane. It was shown that the laser processing by pulsed Nd: YAG laser is an alternative method to the traditional post-growth thermal annealing and can be used not only for local annealing but also for annealing in various depths in the films.

Keywords: Spray pyrolysis; CZTS; Thin films; Nd: YAG laser; Laser processing; Laser irradiation

1. Introduction

Photovoltaic modules based on thin-film technology (TFPV) cover more than 10 % of the global market and, as expected, their share will be increased during the next decade [1]. However, despite their high-efficiency and trust-increasing, there are some disadvantages to using this technology. First of all, these disadvantages are related to the materials used [2]. Nowadays, almost all commercial TFPV's are based on cadmium telluride (CdTe – 21 % of efficiency) or copper gallium indium selenide (CIGS – 22.9 % of efficiency) [3]. They contain the toxic (cadmium), or rare earth (tellurium, indium, and gallium) elements. This fact, in addition to their high-cost value, has significantly limited the wide production of PV-modules based on CdTe and CIGS.

One of the promising alternative materials for fabrication of the high-efficiency and low-cost TFPV is a quaternary semiconductor compound of copper zinc tin sulphide (CZTS) with a kesterite-type phase. In comparison to other compounds, CZTS have significant advantages due to the absence of high-cost chemical elements. Moreover, all composition elements are non-toxic and earth-abundant. These facts, in addition to the excellent optical properties (direct band gap Eg = 1.0-1.5 eV, $\alpha > 10^4$ cm^{-1}), allows CZTS to have a high potential for its used as an absorber layer in TFPV's with a thickness of 1-2 μm [4]. In particular, in the lab area, the current record efficiency of solar cell based on pure CZTS compound is close to 10% [5], and with adding of Se it is 12.6% [6]. In comparison with CdTe and CIGS, such low efficiencies are due to the rapid recombination of the minority charge carriers in the sub-nanosecond regime [7]. In addition, CZTS has a small region of equilibrium state on the phase diagram [8], which creates conditions for the formation of secondary phases. These problems, together with structural defects that occur during growth-process [9], lead to decreasing of photo-conversion efficiency in CZTS-based solar cells. Traditionally, for the healing of structural defects and improving the quality of highly non-oriented polycrystalline

films, the high-temperature thermal annealing technique with the process of sulphurization/selenization is used [10–12]. However, it involves the addition of toxic gas vapour (N_2 + H_2S) or sulphur/selenium powders. Besides, there are always limitations of the maximum annealing temperature, which depended on the substrate material. Therefore, annealing by the scanning laser can be used as an alternative method for improvement of the crystalline quality of as-deposited CZTS thin films without overheating the substrate. Unlike thermal annealing, the technology of laser treatment provides a rapid annealing process of thin films with subsequent recrystallization and improvement of their crystalline quality [13–16]. In addition, the laser annealing technique can significantly reduce the duration of the process and increase the heating temperature of CZTS thin film, while allowing the substrate to remain at a much lower temperature. There are theoretical and experimental studies of the influence of CW diode laser annealing on physical properties of CZTS films [17,18], but the influence of Nd: YAG nanosecond laser irradiation is not well studied yet. In this work, the Nd: YAG laser irradiation process was applied with the aim of improving the quality of polycrystalline CZTS thin films obtained at different deposition temperatures.

2. Experimental details

2.1 CZTS thin film preparation

CZTS thin films were obtained by the spray-pyrolysis method [19] on soda-lime glass (SLG) substrate with deposition temperatures of 523 *K*, 548 *K*, 573 *K*, 598 *K*, and 623 *K* (with increments Δ = 25 *K*). Later on, in the discussion part, they will be denoted as "Sample 1, 2, 3, 4 and 5", respectively.

The initial precursor of CZTS was formed based on distilled water (pH=3) and included the following components: $CuCl_2$ (99%), $ZnCl_2$ (99%), $SnCl_2$ + $2H_2O$ (99%) and CH_4N_2S (99%) with their respective molar ratio 2:1:1.5:8. The initial solution was over-saturated with thiourea in the aim to minimize sulphur deficiency and oxidation processes in the as-deposited

thin films. All reagents and solvent were used in their original form without preliminary purification.

The distance between spray-source and nozzle was 20 cm. The compressed air with the pressure of 2 bar was used as a gas-carrier. In this experiment, the pulsed sputtering technique with a spray-time of 1 s and a pause between spray-cycles of 10 s was used. The overall number of cycles was 100.

2.2 Laser processing

The laser processing of obtained films was carried out using the pulsed nanosecond Nd: YAG laser (Ekspla NL301G with top-hat beam). The scanning method with irradiation velocity of 1.6×10^{-4} m/s was used. The duration of the laser pulse was 4×10^{-9} s, and the beam diameter was d = 1.5 mm. As noted above, CZTS has a direct band gap of 1.5 eV and, thus, the maximal absorption ability for this compound lies in the infrared range of radiation (800-900 nm). In the case of using the Nd: YAG laser with the second harmonic (λ = 532 nm), CZTS films could absorb about 60 % of the green radiation range [20]. As described in [21], under using a nanosecond laser, it is possible to have processes that are on the verge between ablation and surface modification of thin films. Therefore, in order to avoid a direct ablation in the obtained films [22], the value of maximum laser energy was chosen W = 1.24 mJ (minimal value for this laser at λ = 532 nm). The calculated maximum peak intensity of the laser beam was less than I = 17.5 MW/cm^2. The penetration depth of the radiation into a material determines the size of the heated region. This value is the inverse of the absorption coefficient, i.e. $1/\alpha$. In the case of CZTS films, it was 107 nm. Due to the thermal conductivity of the material, the heat-affected zone (HAZ) of the film is increased, and this value can be determined from the following equation:

$$l_t = \sqrt{2Dt}, \quad (1)$$

where D is the thermal diffusivity and t is the pulse duration. In accordance with this equation, the l_t value for a CZTS film with D = 0.2 cm^2/s [23] was about 400 nm. As the laser processing by pulsed Nd: YAG laser creates non-equilibrium conditions with a temperature gradient into the depth of CZTS films, it can be estimated that the laser annealing process has occurred in the HAZ region ($l_t \approx$ 400 nm) of the films. It is worth noting that the laser processing was carried out in the air atmosphere without sulphur incorporation and the samples were cooled down to room temperature naturally after the laser treatment. The overall irradiation time of one sample was 5 minutes. The film obtaining process and laser treatment are shown in Video 1.

2.3 Film characterizations

Thin films were studied in two regimes – as-deposited (condition 1) and after laser processing (condition 2). The film surface microstructure and chemical composition were investigated using atomic force microscope NT-MDT (AFM) and scanning electron microscope FEI Nova NanoSEM 650 Schottky (SEM) with integrated energy dispersive spectroscope Apollo-x (EDS). The height distribution of skewness (S_{SK}) and excess kurtosis (S_{KU}) were computed from 3rd and 4th central moment of data values, respectively. The S_{SK} and S_{KU} values are expressed by the following formulas:

$$Ssk = \frac{\sum_{i=1}^{N}(z_1 - \bar{z})^3/N}{s^3}, \tag{2}$$

$$Sku = \frac{\sum_{i=1}^{N}(z_1 - \bar{z})^4/N}{s^4} - 3, \tag{3}$$

where $\bar{z}$ denotes the mean value, s is the standard deviation, and N is the number of data points. The structural analysis was performed using X-ray diffractometer Rigaku Ultima + (XRD) in the Bragg-Brentano geometry with $K\alpha$ radiation of the copper anode (λ= 1.5406

nm). The average values of coherent scattering regions (CSR, L) and micro-strain (ε) were calculated by Williamson-Hall analysis [24] using the following equation:

$$\beta_{hkl} cos\theta = \frac{k\lambda}{L} + 4\varepsilon\, sin\theta, \tag{4}$$

where β is the physical broadening of the corresponding X-ray lines. Lattice parameters (a, c) of CZTS in both conditions, were determined by the following equations:

$$a = \frac{\lambda}{2\sin\theta}\sqrt{h^2 + k^2 + l^2\left(\frac{a}{c}\right)^2}, \tag{5}$$

$$c = \frac{l}{\sqrt{-\frac{h^2 + k^2}{a^2} + \left(\frac{2sin\theta}{\lambda}\right)^2}}, \tag{6}$$

where λ is the wavelength of X-ray irradiation, θ is the value of Wolf-Bragg angle, h, k, l are the Miller indices. Raman analysis was carried out at room temperature using Raman spectrometer Renishaw InViaV727 in backscattering geometry. The phonon excitation were performed by green (Ar^+, λ = 514.5 nm, grating - 1200 mm^{-1}) and red (He-Ne, λ = 632.8 nm, grating - 1200 mm^{-1}) lasers.

3. Results and discussion

3.1 Surface morphology

The AFM method was used to investigate the influence of laser processing on the surface of CZTS films. AFM images are shown in Fig. 1. It is well-demonstrated (Fig. 1. Condition 1) that, at lower deposition temperatures (samples 1, 2), the surfaces of the films have a structure, which consists of clusters with cracks. During a gradual increase in temperature (samples 3, 4, 5), the surfaces became more homogeneous without the inclusion of significant

large-scale defects and point impurities. After the laser processing (Fig. 1. Condition 2), there agglomeration and coalescence of the material with the formation of round-shaped grains are observed on the surface of each film. The average diameter of these grains is close to 2 μm. It should be noted that the measured height-differences in laser-irradiated films are increased, which indicates the pulling of grains in the direction parallel to the laser beam. The pulling of grains can be associated with the process of ultrafast evaporation of excess sulphur in the films in the presence of a large temperature gradient caused by the pulsed laser irradiation. A possible mechanism is the following. When the sulphur evaporates, vacancies appear in the crystal lattice. Atoms can migrate through these vacancies along the temperature gradient toward the top of the film. It is known as the thermo-gradient effect [25]. It can promote the extension of CZTS grains in the longitudinal direction – the pulling effect. In addition, there are two competing effects: (i) shrinking of the grains due to the loss of material because of the evaporation of S; and (ii) extension of the grains due to a replacement of S atoms by almost twofold larger Cu atoms. As a result of the mentioned here mechanisms, the size and shape of the grains can be changed in accordance with the AFM images in Fig. 1.

Calculations of roughness, skewness and kurtosis parameters for CZTS films in both conditions are shown in Table 1. The change in deposition temperature affects the parameters of mean square roughness (R_q) and average surface roughness (R_a). Samples 4 and 5 in Condition 1 have the minimum values of R_a and R_q. In Condition 2, the values of parameters R_a and R_q are significantly increased in each of the films. The roughness increases due to the process of grains pulling on the surface of thin films. The obtained results have demonstrated a considerable modification of the surface after laser processing.

For a Gaussian height distribution, the statistical theory shows that the ratio of R_a/R_q should be $(2/\pi)^{1/2} \approx 0.8$ [26]. As shown in Table 1, the values of R_q/R_a ratio in both conditions are close to the theoretically predicted value of 0.8. The S_{SK} parameter was calculated to estimate the symmetry of the variations between the high peaks and deep valleys in the

measured plane. For a normal distribution, the value of S_{SK} is zero, and any symmetric surfaces should have a skewness near zero. As it can be seen from Table 1, the S_{SK} values become much smaller and closer to zero after the laser processing. It indicates an improvement in symmetry, that is, the film surface becomes more homogeneous. Negative or positive values of S_{SK} indicate predominant distortion of the surface roughness on the left- or the right-hand side in the measured plane, respectively. The S_{KU} value of the normal distribution is also zero. The S_{KU} parameter is used to measure the distribution of peaks above and below the middle plane. In the case of laser-irradiated films, the S_{KU} values are predominantly become close to zero, except the sample 5. For spiky-surfaces $S_{KU} > 0$; for bumpy-surfaces $S_{KU} < 0$.

In order to confirm the results of AFM measurements, additional measurements by the SEM method for each sample was performed. The micro-images and cross-sections of CZTS films are shown in Fig. 2. The obtained micro-images are well correlated with the AFM images of the corresponding films. At the same time, it is shown in Fig. 2 that the laser-irradiated films have a porous structure. Since the laser processing was carried out in the air, the porous structure may be caused by the rapid evaporation of SO_2 gas, which occurs during the burning process of excess sulphur in the film. The rapid evaporation of SO_2 gas from the volume of CZTS has made its structure porous and has an influence on the height of newly-formed grains. Such a structure of CZTS has a good potential for applications in photocatalytic processes [27], in gas-sensors [28], and as an absorber layer in double-junction solar cells [29].

The size distribution and concentration of newly-formed microparticles have been also studied for each sample, as shown in Fig. 3. As it can be seen from Fig. 3, the size distribution has a Gauss-like form in all cases. Most of the microparticles have an average diameter in the range of 1-2 μm. In samples 4 and 5, a greater agglomeration of newly-formed microparticles with the formation of micro-islands is observed. The diameter of these micro-islands is more

than 2 μm. Such an effect may be associated with changing the chemical concentrations of components in samples, primarily sulphur. These results show that laser processing improved the surface of CZTS thin films and made it more homogeneous with the normal distribution of newly-formed particles throughout the plane.

Previously, we have found [30] that the CZTS thin films, obtained by the spray-pyrolysis method with similar deposition parameters, had a chemical composition close to the stoichiometric value and their further processing by Nd: YAG laser has led to change in concentrations of the components. The results of EDS analysis for each film are shown in Table 2. We observed a tendency of changing in concentrations of compound components during the change in the deposition temperature. At low deposition temperature (samples 1, 2), the film is S-rich, but Cu-poor. Calculation of the atomic concentration ratios for these samples points to stoichiometric violations, which arise during the deposition process. The S-concentration significantly decreased and that of Cu significantly increased after the laser processing. In addition, the ratios of Zn/Sn and Cu+Zn+Sn/S became close to the ideal stoichiometry values for CZTS [31]. In the case of samples 3, 4 and 5, the following situation is observed. The concentrations of each component in the as-deposited films were close to the stoichiometric composition, with minor violations in the case of Zn and Sn. After the laser processing, the S-concentration is decreased and the Zn-concentration is increased. At the same time, the Zn/Sn and Cu+Zn+Sn/S ratios are increased after the laser processing, as shown in Table 2.

From the EDS analysis, one can draw the following conclusions. The S-concentrations in CZTS films decreases with increasing of the deposition temperature. It is due to the low boiling temperature of S (T = 717.75 *K*). The closer is the deposition temperature to the boiling temperature of S, the smaller is the influence of this component on the CZTS formation process. In thin films deposited at low temperature (samples 1, 2), the excess of S has evaporated during the laser processing, which improved the stoichiometric composition.

In the case of high deposition temperature (close to T = 623 *K*), laser processing has led to a decrease of S concentration in a thin film.

3.2 Phase composition

The XRD patterns from as-deposited CZTS films are shown in Fig. 4 (a). The intensive peaks, which correspond to reflections from crystallographic planes of (112), (220), (312) for CZTS (Card no. 00-026-0575) with kesterite-type phase, are observed in diffraction patterns obtained from each of the films. At lower deposition temperatures (samples 1, 2, 3), a peak (200) is observed on the patterns, which also corresponds to the kesterite-type phase of CZTS and indicates a higher crystallization level [12]. Moreover, in films obtained at T = 523 *K* and T = 548 *K*, the peak (112) is more intense and has a low value of full width at half maximum (FWHM). It indicates a better crystalline quality of the films obtained at these deposition temperatures.

After the laser processing (Fig. 4 (b)), the FWHM values are decreased and the intensities of the peaks are increased in radiographs obtained from each sample. The best results were shown in samples 1 and 2. This indicates that the crystalline quality of CZTS thin films is improved by the laser irradiation. It is worth noting that, in all cases after the laser processing, a shift in the position of the peaks (112) and (321) is observed toward smaller 2Θ-angles by 0.1^0. This effect might be caused by the healing of structural defects (dislocations and curvature), which create disruptions in the perfect parallelism of these crystallographic planes.

In order to evaluate the influence of laser processing on CZTS crystal lattice, the parameters *a*, *c*, *L* and ε were calculated. The results are shown in Table 3. The calculated lattice parameters (*a*, *c*) for as-deposited films are close to the reference data of CZTS (Card no. 00-026-0575) with kesterite-type phase, whereas slight deviations are observed in samples 2-5. After the laser processing, the values of lattice parameters (*a*, *c*) are significantly changed and become close to the reference data, especially for sample 2. These changes are shown in Fig. 5. The CSR values of each film after the laser processing are increased. It should be

noted that the CSR values of samples 3-5 are close to the exciton Bohr radius of CZTS. The quantum confinement effect [32,33] can appear in these films.

The calculated micro-strain parameter for as-deposited CZTS films has negative values, except for samples 1 and 2. After the laser processing, micro-strains have only negative values for each of the films. This indicates the appearance of the lattice shrinkage effect [34,35]. However, according to the data in Table 3, one can conclude that the mechanism of the shrinking process of the crystal lattice varies depending on the deposition temperature. As a result, the mechanism by which the laser processing influences the crystal lattice of CZTS is also varied from film to film.

According to the data from EDS analysis, samples 1 and 2 are S-rich and Cu-poor. However, after the laser processing, the chemical concentrations of these components are significantly changed. Therefore, it can be assumed that, in the case of low deposition temperature (in the region close to T = 548 *K*), the laser processing leads to the following shrinking mechanism. Under the action of laser irradiation, the excess of S-atoms is released from the crystal lattice and sulphur positions are occupied by Cu-atoms, which have a larger atomic mass (more than twofold relative to the sulphur). This process is ultrafast and occurs within a time, which is close to the duration of laser beam pulse (4×10^{-9} s) in the processing-point. Consequently, in the case of samples 1 and 2, this process rapidly changes the lattice parameters (*a*, *c*), and it creates conditions for the appearance of the shrinkage effect.

In samples 3, 4 and 5, the lattice shrinkage effect is observed before the laser processing. In this case, the shrinking is caused by the increase of the substrate temperature. The deposition temperature has an influence on the stoichiometry of the composition, especially on the chemical concentration of sulphur. As it can be seen from the data in Table 2, the concentration of sulphur is even more decreased after the laser processing, and a deficit of this component is observed in samples 3, 4 and 5. As a result, the deficit of S-atoms leads to

decreased values of the lattice parameters (*a*, *c*), which causes the shrinkage of the CZTS crystal.

In Fig. 6 (a, b), the Raman spectra are shown, obtained by using a green laser (λ = 514.5 nm). As it can be seen from Fig. 6 (a), spectra from each sample have two main peaks, which are typical for the phonon mode A of CZTS with a kesterite-type structure [36,37]. However, in all cases, except the sample 2, the dominant phonon mode A is located in the range of 333-336 cm^{-1}, which is caused by the stoichiometry violation in as-deposited films [38].

At the same time, the Raman spectra of laser-irradiated films (Fig. 6 (b)) significantly differs from Raman spectra of as-deposited films (Fig. 6 (a)). A shift of the dominant peak toward a smaller value, i.e., to 328 cm^{-1}, is observed after the laser processing. The peak intensities of the laser-irradiated films are increased more than twofold and the values of FWHM are decreased. On the one hand, this result suggests the improvement of crystalline quality in the laser-irradiated films [39]. However, on the other hand, it may indicate an appearance of local inhomogeneities in the crystal lattice caused by the shrinkage effect. These inhomogeneities can lead to statistical disordering and changes of the crystal symmetry from ordered $I\bar{4}$ to disordered kesterite $I\bar{4}2m$ [40–42]. In the case of our work, this question will remain open and requires a more detailed study.

In order to achieve conditions close to resonance [36] and to increase the sensitivity of secondary phase detection [43], a red laser (λ = 632.8 nm) was used to measure the Raman spectra. The obtained spectra are shown in Fig. 7 (a, b). As in the case of the green laser, peaks were found in the spectra of each sample at frequencies of 338 cm^{-1} and 296 cm^{-1}, corresponding to the main phonon mode A. However, at a frequency of 376 cm^{-1}, peaks are observed in the Raman spectra, which correspond to the phonon mode E/B [44]. The intensity of peaks had the highest values in samples 1 and 2.

The differences in the spectra, that were obtained with using the green and the red laser, point to certain heterogeneities of CZTS formation inside thin films. As shown in Fig. 7 (b),

the Raman spectra after laser processing are smoothened out and become more similar to the Raman spectra obtained with the green laser (Fig. 6 (b)). Moreover, the peak corresponding to the phonon mode E/B completely disappears from the spectra. Since the penetration depth of the red laser into CZTS film is slightly larger (≈167 nm) than that of the green laser, it can be concluded that the laser processing contributes to the formation of a more homogeneous structure in the HAZ area. In the Raman spectra obtained after laser processing (Fig. 7(b)), the highest intensity of the main peak was observed for sample 1. This result is well correlated with the previous XRD measurements. The results of the Raman analysis show that each sample before and after the laser processing has a single-phase kesterite-type structure of CZTS.

Conclusions

As a result of this work, the CZTS thin films were obtained by the spray-pyrolysis method at different deposition temperatures. It was found that low deposition temperatures (T = 523-573 *K*) create conditions for the formation of clusters with cracks on the surface of the films. With a gradual increase of the temperature up to T = 623 *K*, the surface became smooth without visible large-scale defects and point impurities. The laser processing has modified the surface considerably and has improved the chemical stoichiometric composition of the films. The laser-irradiated films have a porous structure with the round-shaped grains on the surface. The newly formed grains increased the surface roughness, but, at the same time, improved the symmetry, making the surface more homogeneous throughout the plane. Cracks on the surface of thin films were healed after the laser processing. The results of phase analysis have confirmed the fact that each sample had a single phase of CZTS with a kesterite-type structure both before and after the laser processing. Thin films deposited at T = 523-573 *K* have a higher crystallization level than films deposited at T = 598-623 *K*. The laser processing contributed to the formation of a more homogeneous structure in the HAZ area. In addition,

an improvement of crystallinity of CZTS thin films was observed. It was found that the lattice shrinkage effect takes place, having two mechanisms of formation.

The obtained results show that the laser processing significantly improves the surface morphology, stoichiometric composition, structure and crystalline quality of the irradiated layer in CZTS films. This process is ultrafast and can be used as an alternative to the traditional technology of thermal annealing or as a process for surface-modification of thin semiconductor films.

Acknowledgment

This research was supported by the Ministry of Education and Science of Ukraine (Grant numbers 0117U003929, 0118U003576, 0116U06813) and the Latvian State Education Development Agency (individual grant for A. Shamardin, Nr.1.-50.3/ 3845).

Reference

[1] A. Jäger-Waldau, PV Status Report 2017, EUR 28817 EN, Publications Office of the European Union, Luxembourg, JRC108105, 2017. doi:10.2760/452611.

[2] A. Feltrin, A. Freundlich, Material considerations for terawatt level deployment of photovoltaics, Renew. Energy. 33 (2008) 180–185. doi:10.1016/j.renene.2007.05.024.

[3] M.A. Green, Y. Hishikawa, E.D. Dunlop, D.H. Levi, J. Hohl-Ebinger, A.W.Y. Ho-Baillie, Solar cell efficiency tables (version 52), Prog. Photovoltaics Res. Appl. 26 (2018) 427–436. doi:10.1002/pip.3040.

[4] D.B. Mitzi, O. Gunawan, T.K. Todorov, K. Wang, S. Guha, Solar Energy Materials & Solar Cells The path towards a high-performance solution-processed kesterite solar cell $, Sol. Energy Mater. Sol. Cells. 95 (2011) 1421–1436. doi:10.1016/j.solmat.2010.11.028.

[5] M.A. Green, Y. Hishikawa, E.D. Dunlop, D.H. Levi, J. Hohl-Ebinger, A.W.Y. Ho-

Baillie, Solar cell efficiency tables (version 51), Prog. Photovoltaics Res. Appl. 26 (2018) 3–12. doi:10.1002/pip.2978.

[6] W. Wang, M.T. Winkler, O. Gunawan, T. Gokmen, T.K. Todorov, Y. Zhu, D.B. Mitzi, Device characteristics of CZTSSe thin-film solar cells with 12.6% efficiency, Adv. Energy Mater. 4 (2014) 1–5. doi:10.1002/aenm.201301465.

[7] J. Márquez, H. Stange, C.J. Hages, N. Schaefer, S. Levcenko, S. Giraldo, E. Saucedo, K. Schwarzburg, D. Abou-Ras, A. Redinger, M. Klaus, C. Genzel, T. Unold, R. Mainz, Chemistry and Dynamics of Ge in Kesterite: Toward Band-Gap-Graded Absorbers, Chem. Mater. 29 (2017) 9399–9406. doi:10.1021/acs.chemmater.7b03416.

[8] G. Altamura, J. Vidal, Impact of Minor Phases on the Performances of CZTSSe Thin-Film Solar Cells, Chem. Mater. 28 (2016) 3540–3563. doi:10.1021/acs.chemmater.6b00069.

[9] M. Kumar, A. Dubey, N. Adhikari, S. Venkatesan, Q. Qiao, Strategic review of secondary phases, defects and defect-complexes in kesterite CZTS-Se solar cells, Energy Environ. Sci. 8 (2015) 3134–3159. doi:10.1039/c5ee02153g.

[10] M.G. Sousa, A.F. Da Cunha, P.A. Fernandes, J.P. Teixeira, R.A. Sousa, J.P. Leitão, Effect of rapid thermal processing conditions on the properties of Cu2ZnSnS4thin films and solar cell performance, Sol. Energy Mater. Sol. Cells. 126 (2014) 101–106. doi:10.1016/j.solmat.2014.03.043.

[11] M.A. Olgar, J. Klaer, R. Mainz, L. Ozyuzer, T. Unold, Cu2ZnSnS4-based thin films and solar cells by rapid thermal annealing processing, Thin Solid Films. 628 (2017) 1–6. doi:10.1016/j.tsf.2017.03.008.

[12] R. Chen, J. Fan, H. Li, C. Liu, Y. Mai, Efficiency enhancement of Cu2ZnSnS4 solar cells via surface treatment engineering, R. Soc. Open Sci. 5 (2018) 171163. doi:10.1098/rsos.171163.

[13] H.J. Meadows, A. Bhatia, V. Depredurand, J. Guillot, D. Regesch, A. Malyeyev, D. Colombara, M.A. Scarpulla, S. Siebentritt, P.J. Dale, Single second laser annealed CuInSe2 semiconductors from electrodeposited precursors as absorber layers for solar cells, J. Phys. Chem. C. 118 (2014) 1451–1460. doi:10.1021/jp409804s.

[14] A. Voznyi, V. Kosyak, P. Onufrijevs, L. Grase, J. Vecstaudža, A. Opanasyuk, A. Medvid, Laser-induced SnS2-SnS phase transition and surface modification in SnS2 thin films, J. Alloys Compd. (2016). doi:10.1016/j.jallcom.2016.07.103.

[15] M.Y. Zhang, Q. Nian, Y. Shin, G.J. Cheng, Direct pulsed laser crystallization of nanocrystals for absorbent layers in photovoltaics: Multiphysics simulation and experiment, J. Appl. Phys. 113 (2013). doi:10.1063/1.4805039.

[16] B.J. Simonds, V. Palekis, M.I. Khan, C.S. Ferekides, M.A. Scarpulla, Pulsed UV laser annealing of polycrystalline CdTe, Laser Mater. Process. Sol. Energy Devices II. Proc. SPIE (2013) 882607--. doi:10.1117/12.2024437.

[17] M.S. Ahmmed, E.R. Hawkes, M.A. Green, Diode laser annealing of CZTS thin film solar cells, 2015 IEEE 42nd Photovolt. Spec. Conf. (2015) 1–5. doi:10.1109/PVSC.2015.7355800.

[18] N. Song, J. Huang, M.A. Green, X. Hao, Diode laser annealing on sputtered epitaxial Cu2ZnSnS4 thin films, Phys. Status Solidi - Rapid Res. Lett. 11 (2017) 1700033. doi:10.1002/pssr.201700033.

[19] O. V. Diachenko, A.S. Opanasuyk, D.I. Kurbatov, N.M. Opanasuy, O.K. Kononov, D. Nam, H. Cheong, Surface morphology, structural and optical properties of MgO films obtained by spray pyrolysis technique, Acta Phys. Pol. A. 130 (2016) 805–810. doi:10.12693/APhysPolA.130.805.

[20] A.J. Nelson, M. Danailov, L. Gregoratti, M. Marsi, M. Kiskinova, Scanning

photoelectron microscopy study of the laser-induced transformations of polycrystalline CdTe films, J. Appl. Phys. 87 (2000) 3520–3525. doi:10.1063/1.372375.

[21] B.J. Simonds, H.J. Meadows, S. Misra, C. Ferekides, P.J. Dale, M.A. Scarpulla, Laser processing for thin film chalcogenide photovoltaics: a review and prospectus, J. Photonics Energy. 5 (2015) 050999. doi:10.1117/1.JPE.5.050999.

[22] S.A. Vanalakar, G.L. Agawane, S.W. Shin, M.P. Suryawanshi, K. V. Gurav, K.S. Jeon, P.S. Patil, C.W. Jeong, J.Y. Kim, J.H. Kim, A review on pulsed laser deposited CZTS thin films for solar cell applications, J. Alloys Compd. 619 (2015) 109–121. doi:10.1016/j.jallcom.2014.09.018.

[23] S. Adachi, Introduction, John Wiley & Sons, Chichester, UK, 2015. doi:10.1002/9781119052814.ch1.

[24] V. Mote, Y. Purushotham, B. Dole, Williamson-Hall analysis in estimation of lattice strain in nanometer-sized ZnO particles, J. Theor. Appl. Phys. 6 (2012) 6. doi:10.1186/2251-7235-6-6.

[25] A. Medvids, L. Grase, P. Onufrijevs, H. Mimura, V. Yukhymchuk, G. Mezinskis, Two-stage mechanism of Zn nanoparticles formation in ZnO crystal by Nd:YAG laser radiation, 14 (2017). doi:10.1002/pssc.201700038.

[26] T.R. Thomas, Rough Surfaces, Second, Imperial College Press, 1998. doi:10.1142/p086.

[27] A. Apostolopoulou, S. Mahajan, R. Sharma, E. Stathatos, Novel development of nanocrystalline kesterite Cu2ZnSnS4 thin film with high photocatalytic activity under visible light illumination, J. Phys. Chem. Solids. 112 (2018) 37–42. doi:10.1016/j.jpcs.2017.09.005.

[28] K. V. Gurav, S.W. Shin, U.M. Patil, P.R. Deshmukh, M.P. Suryawanshi, G.L. Agawane, S.M. Pawar, P.S. Patil, J.Y. Lee, C.D. Lokhande, J.H. Kim, Cu2ZnSnS4(CZTS)-

based room temperature liquefied petroleum gas (LPG) sensor, Sensors Actuators, B Chem. 190 (2014) 408–413. doi:10.1016/j.snb.2013.08.064.

[29] P. Dai, G. Zhang, Y. Chen, H. Jiang, Z. Feng, Z. Lin, J. Zhan, Porous copper zinc tin sulfide thin film as photocathode for double junction photoelectrochemical solar cells, Chem. Commun. 48 (2012) 3006–3008. doi:10.1039/c2cc17652a.

[30] A. V. Shamardin, A.S. Opanasyuk, D.I. Kurbatov, A. Medvids, The effect of laser processing on the structural characteristics and elemental composition of CZTS thin film obtained by spray pyrolysis method, in: 2nd Int. Conf. Inf. Telecommun. Technol. Radio Electron. UkrMiCo 2017 - Proc., 2017: pp. 1–4. doi:10.1109/UkrMiCo.2017.8095397.

[31] S. Chen, A. Walsh, X.G. Gong, S.H. Wei, Classification of lattice defects in the kesterite Cu2ZnSnS4 and Cu2ZnSnSe4 earth-abundant solar cell absorbers, Adv. Mater. 25 (2013) 1522–1539. doi:10.1002/adma.201203146.

[32] J.-J. Wang, P. Liu, K.M. Ryan, A facile phosphine-free colloidal synthesis of Cu2SnS3 and Cu2ZnSnS4 nanorods with a controllable aspect ratio, Chem. Commun. 51 (2015) 13810–13813. doi:10.1039/C5CC04979B.

[33] J.H.N. Tchognia, Y. Arba, B. Hartiti, A. Ridah, J.M. Ndjaka, P. Thevenin, Effect of sulfurization time on properties of Cu2ZnSnS4thin films obtained by sol–gel deposited precursors, Opt. Quantum Electron. 48 (2016) 1–7. doi:10.1007/s11082-016-0424-2.

[34] J. He, L. Sun, N. Ding, H. Kong, S. Zuo, S. Chen, Y. Chen, P. Yang, J. Chu, Single-step preparation and characterization of Cu2ZnSn(SxSe1-x)4thin films deposited by pulsed laser deposition method, J. Alloys Compd. 529 (2012) 34–37. doi:10.1016/j.jallcom.2012.03.065.

[35] J. Li, H. shen, Y. Li, H. Yao, W. Wang, W. Wu, Z. Ren, Influence of sulfurization pressure on structural and electrical property of Cu2ZnSnS4thin film and solar cell, J. Mater.

Sci. Mater. Electron. 27 (2016) 8688–8692. doi:10.1007/s10854-016-4890-x.

[36] M. Guc, S. Levcenko, I.V. Bodnar, V. Izquierdo-roca, X. Fontane, L.V. Volkova, E. Arushanov, A. Pérez-Rodríguez, Polarized Raman scattering study of kesterite type Cu_2ZnSnS_4 single crystals, Sci. Rep. 5 (2016) 19414/1-7. doi:10.1038/srep19414.

[37] P.A. Fernandes, P.M.P. Salomé, A.F. Da Cunha, Study of polycrystalline Cu2ZnSnS4films by Raman scattering, J. Alloys Compd. 509 (2011) 7600–7606. doi:10.1016/j.jallcom.2011.04.097.

[38] R. Caballero, E. Garcia-Llamas, J.M. Merino, M. Leon, I. Babichuk, V. Dzhagan, V. Strelchuk, M. Valakh, Non-stoichiometry effect and disorder in Cu2ZnSnS4 thin films obtained by flash evaporation: Raman scattering investigation, Acta Mater. 65 (2014) 412–417. doi:10.1016/j.actamat.2013.11.010.

[39] J.J.S. Scragg, L. Choubrac, A. Lafond, T. Ericson, C. Platzer-Björkman, A low-temperature order-disorder transition in Cu2ZnSnS4 thin films, Appl. Phys. Lett. 104 (2014) 041911. doi:10.1063/1.4863685.

[40] X. Fontané, V. Izquierdo-roca, E. Saucedo, S. Schorr, V.O. Yukhymchuk, M.Y. Valakh, A. Pérez-rodríguez, J.R. Morante, Vibrational properties of stannite and kesterite type compounds : Raman scattering analysis of Cu2(Fe,Zn)SnS4, 539 (2012) 190–194. doi:10.1016/j.jallcom.2012.06.042.

[41] M.Y. Valakh, O.F. Kolomys, S.S. Ponomaryov, V.O. Yukhymchuk, I.S. Babichuk, E. Saucedo, J.R. Morante, S. Schorr, I. V Bodnar, Raman scattering and disorder effect in Cu2ZnSnS4, 4 (2013) 1–4. doi:10.1002/pssr.201307073.

[42] S. Schorr, G. Gonzalez-Aviles, In-situ investigation of the structural phase transition in kesterite, Phys. Status Solidi. 206 (2009) 1054–1058. doi:10.1002/pssa.200881214.

[43] E. Garcia-Llamas, J.M. Merino, R. Serna, X. Fontané, I.A. Victorov, A. Pérez-

Rodríguez, M. León, I. V. Bodnar, V. Izquierdo-Roca, R. Caballero, Wide band-gap tuning Cu2ZnSn1−xGexS4 single crystals: Optical and vibrational properties, Sol. Energy Mater. Sol. Cells. 158 (2016) 147–153. doi:10.1016/j.solmat.2015.12.021.

[44] D.L. Mai, H.J. Park, I.H. Choi, Growth of Cu2ZnSnS4 crystals by the directional freezing method with an induction heater, J. Cryst. Growth. 402 (2014) 104–108. doi:10.1016/j.jcrysgro.2014.05.014.

Figure captions

Video 1. CZTS thin film deposition process and further laser processing.

Fig. 1. Two-dimensional (2D) AFM images from CZTS films before (Condition 1) and after (Condition 2) the laser processing.

Fig. 2. SEM micro-images and cross-sections of CZTS films before (Condition 1) and after (Condition 2) the laser processing.

Fig. 3. 3D size distribution of newly-formed microparticles.

Fig. 4. XRD patterns of CZTS films before (a) and after (b) the laser processing.

Fig. 5. Dependence of the lattice parameters (a, c) on the deposition temperature and laser processing.

Fig. 6. μ-Raman analysis of as-deposited (a) and laser-irradiated (b) thin films of CZTS with excitation by a green laser (λ = 514.5 nm).

Fig. 7. μ-Raman analysis of as-deposited (a) and laser-annealed (b) thin films of CZTS with excitation by a red laser (λ = 632.8 nm).

Table 1. Calculation of roughness, skewness and excess kurtosis parameters of CZTS thin films before and after the laser processing

Condition	T, *K*	Sample	R_q, nm	R_a, nm	R_a/R_q	S_{SK}	S_{KU}
1	523	1	770	609	0.79	1.005	0.7040
2			837	661	0.79	0.5887	0.2309
1	548	2	700	543	0.78	1.024	1.089
2			930	740	0.80	0.4207	0.3946
1	573	3	340	287	0.84	0.8289	0.6650
2			518	431	0.83	0.01587	-0.6534
1	598	4	287	226	0.79	0.8021	0.7906
2			459	382	0.83	-0.1646	-0.5339
1	623	5	130	105	0.81	0.3987	0.1436
2			462	384	0.83	-0.1389	-0.3808

Table 2. Chemical compositions of CZTS thin films

Condition	T, *K*	Sample	*Cu* (at.%)	*Zn* (at.%)	*Sn* (at.%)	*S* (at.%)	*Cu*/(*Zn*+*Sn*)	*Zn*/*Sn*	M/*S*
1	523	1	13.9	14.4	14.6	57.1	0.48	0.98	0.75
2			23.2	14.5	12.6	49.7	0.86	1.15	1.01
1	548	2	16.4	11.2	15.6	56.8	0.61	0.72	0.76
2			23.3	13.8	13.7	49.2	0.85	1.00	1.03
1	573	3	21.6	10.5	16.4	51.5	0.80	0.64	0.94
2			24.3	12.7	15.2	47.8	0.87	0.83	1.09
1	598	4	22.7	12.9	15.7	48.7	0.79	0.82	1.05
2			24.5	14.5	14.4	46.6	0.85	1.00	1.15
1	623	5	23.9	12.1	15.9	48.1	0.85	0.76	1.08
2			23.4	14.9	15.3	46.4	0.78	0.97	1.16

Note: M = *Cu* + *Zn* + *Sn*

Table 3. Calculation of CZTS films structural properties

Condition	T, *K*	Sample	Lattice parameters, nm				$L_{(W-H)}$, nm	$\varepsilon_{(W-H)}$
			a	*c*	*c/2a*	*V*		
1	523	1	0.5428	1.1079	1.0205	0.3264	4.5	0.0049
2			0.5422	1.0738	0.9902	0.3157	5.7	-
1	548	2	0.5408	1.0521	0.9727	0.3077	4	0.0027
2			0.5427	1.0849	0.9995	0.3195	5.3	-
1	573	3	0.5435	1.1328	1.0421	0.3346	3	-
2			0.5415	1.0525	0.9718	0.3086	4.1	-
1	598	4	0.5441	1.1328	1.0410	0.3354	2.7	-
2			0.5424	1.0848	1	0.3192	3.3	-
1	623	5	0.5414	1.0846	1.0017	0.3179	2.9	-
2			0.5428	1.0963	1.0099	0.3230	3.8	-
Reference	$a = 0.5427$ nm, $c = 1.0848$ nm, $c/2a = 0.9994$, $V = 0.3195$ nm^3 (Card no. 00-026-0575)							

Note: Condition 1 – as-deposited films; Condition 2 – laser irradiated films

Highlights

1. CZTS thin films had a single phase with a kesterite-type structure both before and after the laser processing.

2. After the laser processing, the surface of thin films had a porous structure with a homogeneous distribution of newly-formed round-shaped grains throughout the plane.

3. Cracks on the surface of thin films were healed after the laser processing.

4. The laser processing significantly improved the surface morphology, stoichiometric composition, structure and crystalline quality of the irradiated layer in CZTS thin films.

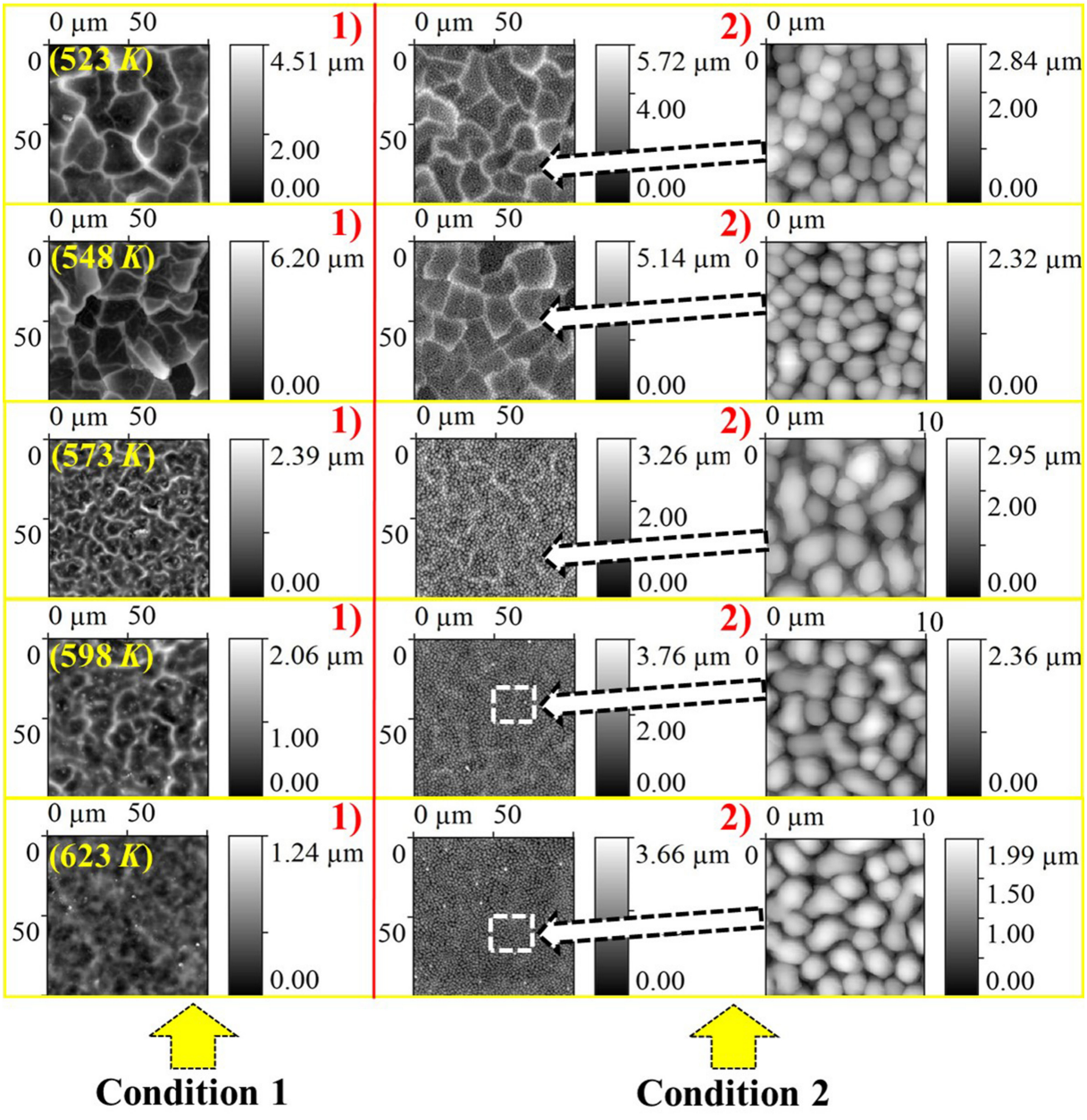
0 μm 50
0
50
(523 K)
1)
4.51 μm
2.00
0.00
2)
5.72 μm
4.00
0.00
0 μm
2.84 μm
(548 K)
6.20 μm
5.14 μm
2.32 μm
(573 K)
2.39 μm
3.26 μm
2.95 μm
10
(598 K)
2.06 μm
1.00
3.76 μm
2.36 μm
(623 K)
1.24 μm
3.66 μm
1.99 μm
1.50
Condition 1
Condition 2

Figure 1

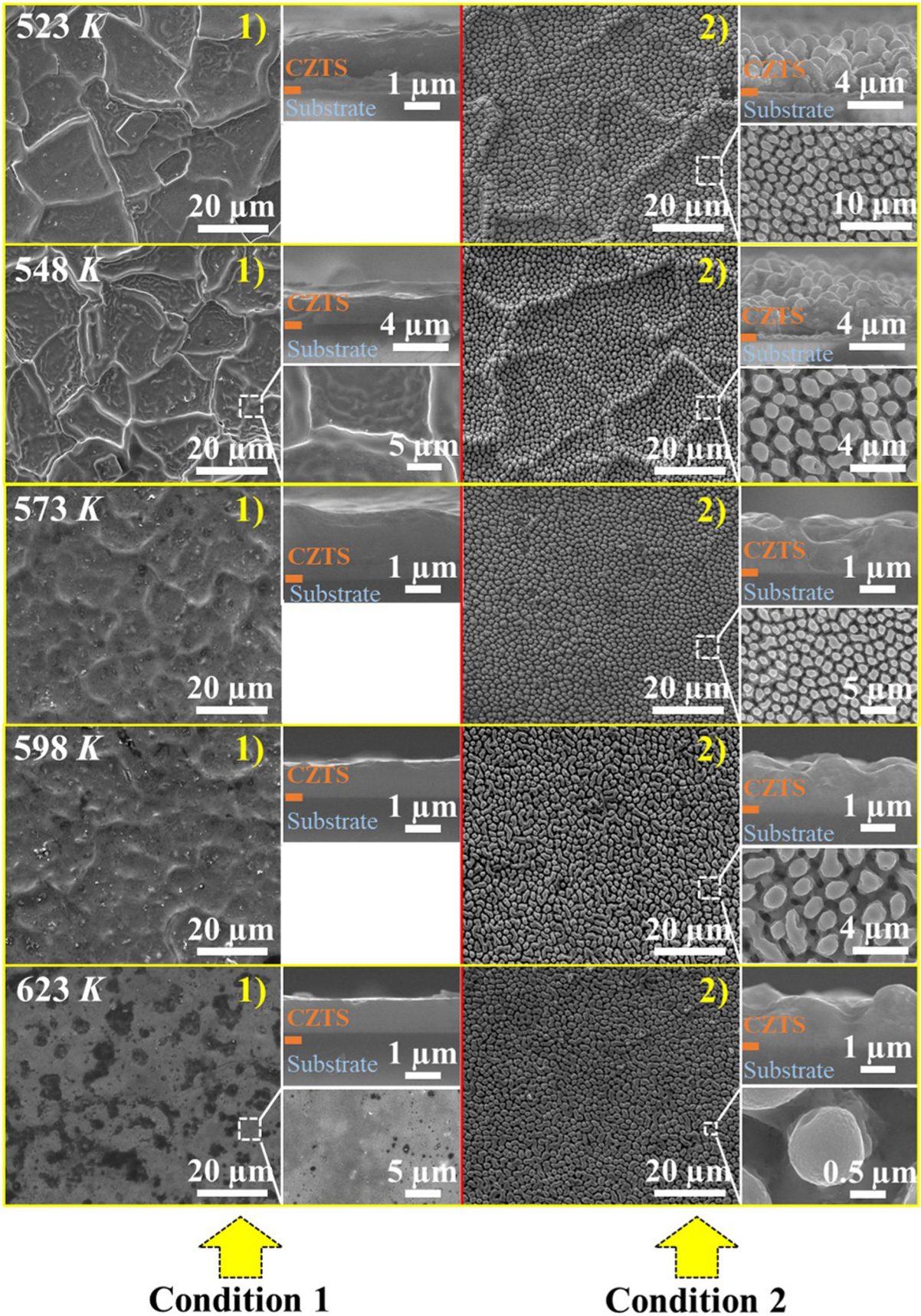
523 K
1)
20 μm
CZTS
Substrate
1 μm
2)
20 μm
CZTS
Substrate
4 μm
10 μm
548 K
1)
20 μm
CZTS
Substrate
4 μm
5 μm
2)
20 μm
CZTS
Substrate
4 μm
4 μm
573 K
1)
20 μm
CZTS
Substrate
1 μm
2)
20 μm
CZTS
Substrate
1 μm
5 μm
598 K
1)
20 μm
CZTS
Substrate
1 μm
2)
20 μm
CZTS
Substrate
1 μm
4 μm
623 K
1)
20 μm
CZTS
Substrate
1 μm
5 μm
2)
20 μm
CZTS
Substrate
1 μm
0.5 μm
Condition 1
Condition 2

Figure 2

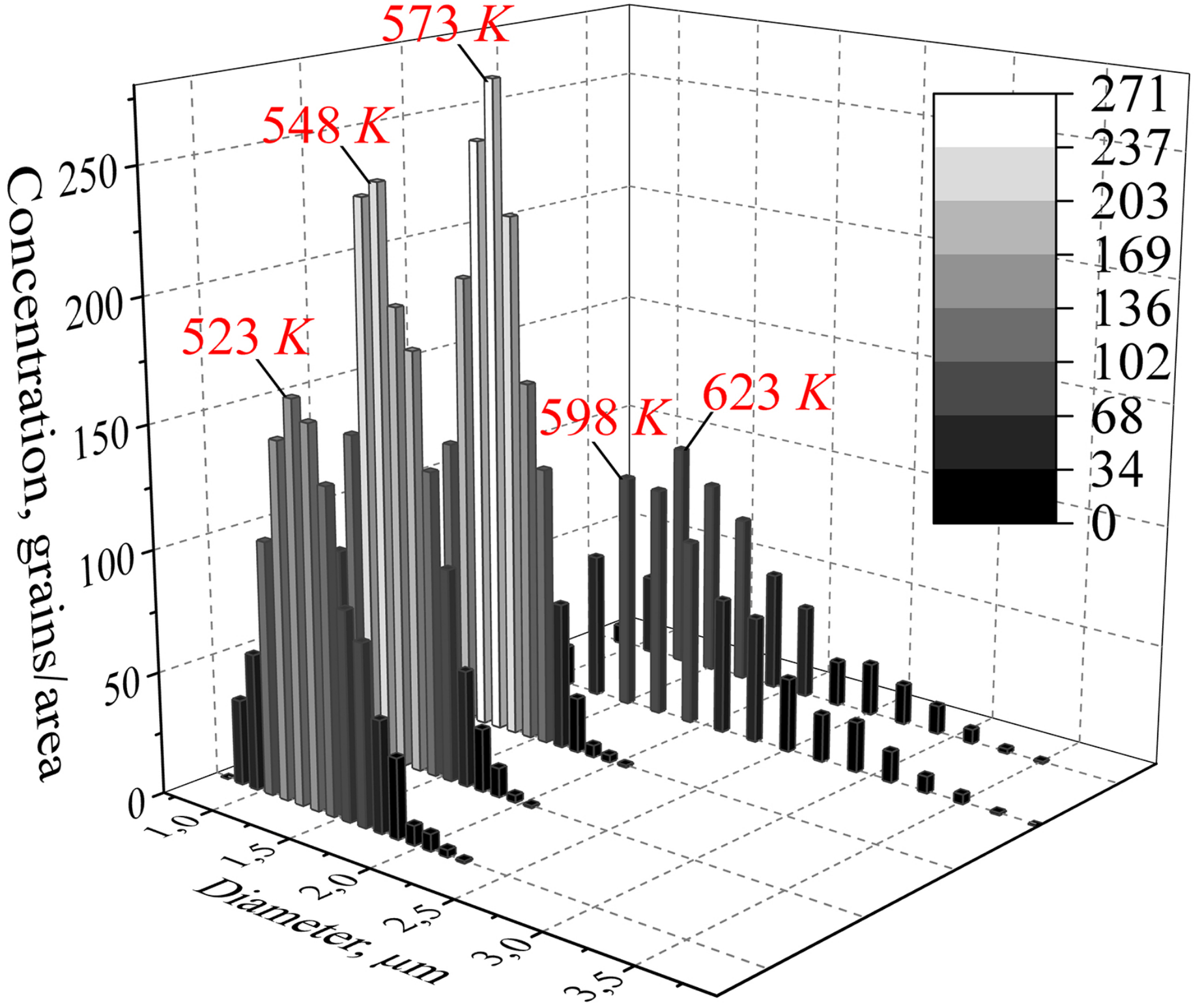
573 K
548 K
523 K
598 K
623 K
Concentration, grains/area
0
50
100
150
200
250
Diameter, μm
1,0
1,5
2,0
2,5
3,0
3,5
271
237
203
169
136
102
68
34
0

Figure 3

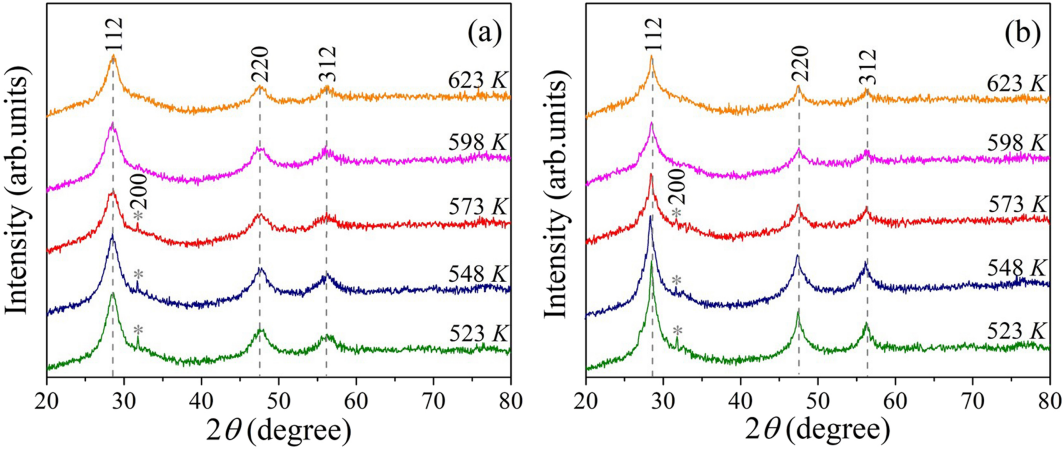
(a)
(b)
112
220
312
200
623 K
598 K
573 K
548 K
523 K
Intensity (arb.units)
2θ (degree)
20
30
40
50
60
70
80

Figure 4

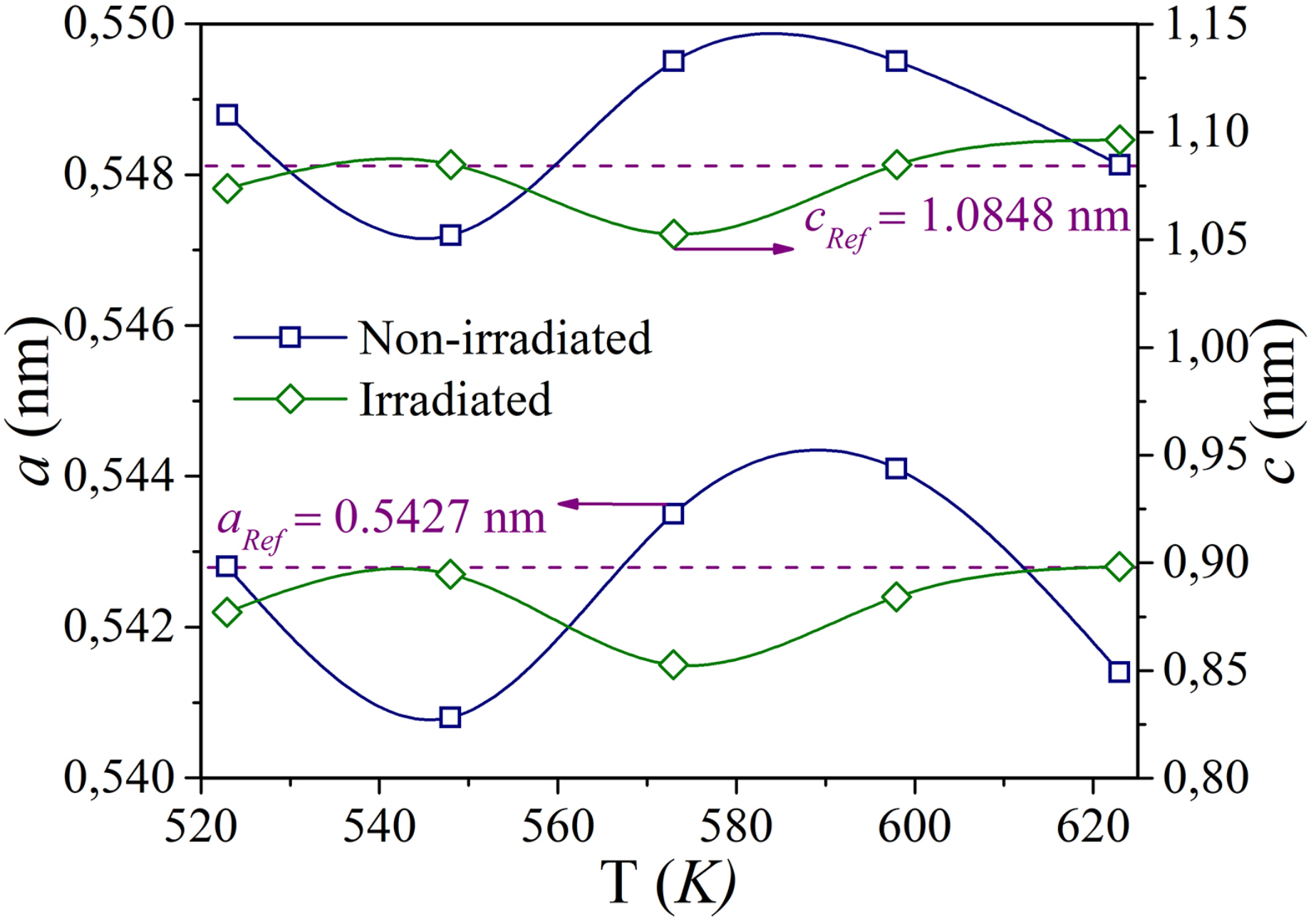
0,550
0,548
0,546
0,544
0,542
0,540
a (nm)
1,15
1,10
1,05
1,00
0,95
0,90
0,85
0,80
c (nm)
520
540
560
580
600
620
T (K)
Non-irradiated
Irradiated
c_{Ref} = 1.0848 nm
a_{Ref} = 0.5427 nm

Figure 5

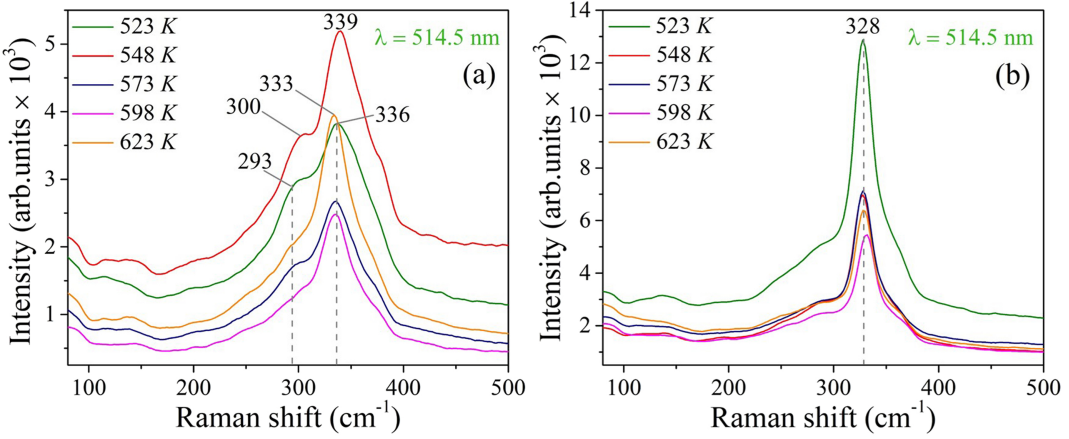
523 K
548 K
573 K
598 K
623 K
λ = 514.5 nm
(a)
339
333
300
336
293
Intensity (arb.units × 10^3)
Raman shift (cm^-1)
523 K
548 K
573 K
598 K
623 K
λ = 514.5 nm
(b)
328
Intensity (arb.units × 10^3)
Raman shift (cm^-1)

Figure 6

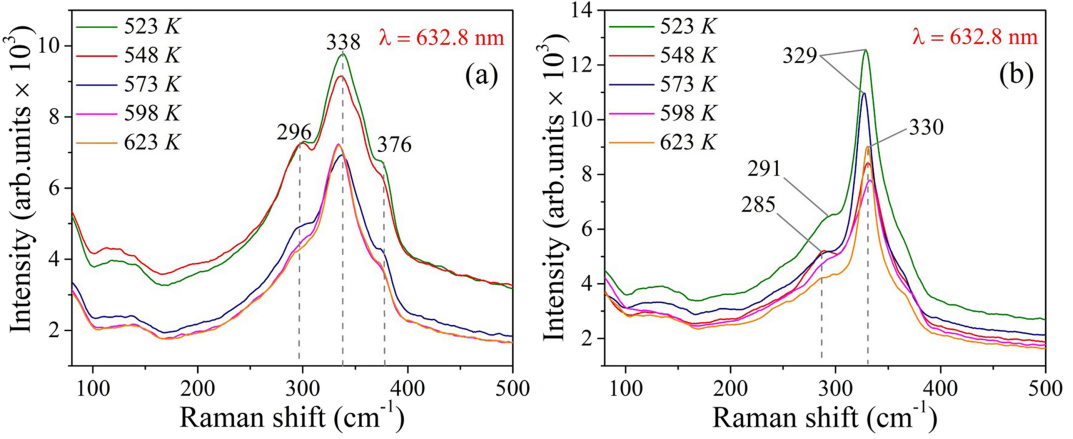
523 K
548 K
573 K
598 K
623 K
λ = 632.8 nm
(a)
338
296
376
Intensity (arb.units × 10^3)
Raman shift (cm^-1)
(b)
329
330
291
285

Figure 7